Supporting information for:

Accelerating Post-SELEX Aptamer Engineering using Exonuclease Digestion

Juan Canoura, Haixiang Yu, Obtin Alkhamis, Daniel Roncancio, Rifat Farhana and Yi Xiao*

Department of Chemistry and Biochemistry, Florida International University, 11200 SW 8th Street, Miami, FL, USA, 33199.

*Corresponding author: yxiao2@fiu.edu

EXPERIMENTAL SECTION

Polyacrylamide gel electrophoresis (PAGE) analysis of digestion products. Digestion products were analyzed by denaturing PAGE by combining 5 µL of sample with 10 µL of formamide loading buffer (75% formamide, 10% glycerol, 0.125% SDS, 10 mM EDTA, and 0.15% (w/v) xylene cyanol), and then loading 6 µL of each sample into the wells of a 15% denaturing PAGE gel. Separation was carried out at 6 V/cm for 30 mins followed by 25 V/cm for 3 h in 0.5 × TBE. The gel was stained with 1× SYBR Gold solution for 25 mins and imaged using a ChemiDoc MP Image system (Bio-Rad).

Circular dichroism (CD) spectroscopy. All CD experiments were performed at room temperature in 10 mM Tris-HCl, 20 mM NaCl, and 1.5 mM $MgCl_2$ (pH 7.4) using a Jasco J-815 circular dichroism spectropolarimeter. Prior to each experiment, 1.5 µM aptamer (final concentration) was heated to 95 °C for 10 mins in Tris buffer and then immediately cooled on ice. Afterwards, salt was added. Blank solution or ADE was then added to aptamer solution to a final concentration of 25, or 50 µM. 300 µL of sample was transferred into a 1 cm quartz cuvette (Hellma Analytics) for measurements. The following parameters were used: 210 to 310 nm scan range, 50 nm/min scan speed, 5 mdeg sensitivity, 4 s response time, 1 nm bandwidth, and 5 accumulation scans total. Reference spectra of reaction buffer without aptamer were taken with 0, 25, or 50µM ADE. Reference spectra were subtracted from CD spectra collected in the presence of aptamer with ADE. To correct for differences in nucleotide length, the CD signal was converted to the mean residue molar extinction coefficient ($\Delta\varepsilon_{MR}$).[1]

Electrochemical measurements. Electrochemical measurements were taken using a CHI 760 bi-potentiostat (CH Instruments). Prior to measurement, the electrodes were incubated in 10% SDS for 15 mins followed by a 20s DI water rinse, after which the electrode was stored in 10 mM Tris-HCl, 20 mM NaCl, and 1.5 mM $MgCl_2$ (pH 7.4) reaction buffer. All measurements were performed at room temperature using a three-electrode system, including an aptamer-modified gold working electrode, a platinum wire counter electrode, and an Ag/AgCl (3M KCl) reference electrode (CH Instruments) in a 2 mL electrochemical cell. Square-wave voltammetry was used for sensor measurements, and voltammograms were collected from -0.1 to -0.4 V (vs Ag/AgCl) using a frequency of 200 Hz with an amplitude of 25 mV. Calibration curves were collected by challenging the E-AB sensors with varying concentrations of ligand dissolved in reaction buffer or 50% fetal bovine serum diluted in reaction buffer. The sensor was equilibrated for 1 min at each target concentration prior to measurements. Signal gain (SG) was calculated using Eq. (2):

$$SG = [(I - I_0)/I_0] \times 100 \quad (2)$$

where I_0 and I are the peak currents obtained in the absence and presence of target, respectively. Cross-reactivity of the sensor to AMP, ADP, ATP, GTP, CTP and UTP was calculated relative to the signal gain produced by 100 μM ADE.

Reference:

(1) Fasman, G. D. *Circular Dichroism and the Conformational Analysis of Biomolecules.* Salmon Tower Building, N.Y.: Springer, **1996**.

Table S1. All oligonucleotide sequences used in this work.

Sequence ID	Sequence (5'–3')
OBAwt	GGG GTG AAA CGG GTC CCG
OBA1	CGG GGT GAA ACG GGT CCC G
OBA2	GGG GCG AAG CGG GTC CCG
OBA3	CGG GGC GAA GCG GGT CCC G
OBA4	GGG GTG AAA CGG TCC CG
OBA5	CCG GGG CGA AGC GGG TCC CGG
OBA6	GCG GGG CGA AGC GGG TCC CGC
ATPwt	CGC ACC TGG GGG AGT ATT GCG GAG GAA GGT GCG
G10A	CGC ACC TGG AGG AGT ATT GCG GAG GAA GGT GCG
G10T	CGC ACC TGG TGG AGT ATT GCG GAG GAA GGT GCG
G10C	CGC ACC TGG CGG AGT ATT GCG GAG GAA GGT GCG
A13T	CGC ACC TGG GGG TGT ATT GCG GAG GAA GGT GCG
A13G	CGC ACC TGG GGG GGT ATT GCG GAG GAA GGT GCG
A13C	CGC ACC TGG GGG CGT ATT GCG GAG GAA GGT GCG
A23T	CGC ACC TGG GGG AGT ATT GCG GTG GAA GGT GCG
A23T-30	CGC ACC TGG GGG AGT ATT GCG GTG GAA GGT
A23T-29	CGC ACC TGG GGG AGT ATT GCG GTG GAA GG
A23G	CGC ACC TGG GGG AGT ATT GCG GGG GAA GGT GCG
A23C	CGC ACC TGG GGG AGT ATT GCG GCG GAA GGT GCG
A26T	CGC ACC TGG GGG AGT ATT GCG GAG GTA GGT GCG
A26G	CGC ACC TGG GGG AGT ATT GCG GAG GGA GGT GCG
A26C	CGC ACC TGG GGG AGT ATT GCG GAG GCA GGT GCG
G10T-A23G	CGC ACC TGG TGG AGT ATT GCG GGG GAA GGT GCG
G10T-A23G-30	CGC ACC TGG TGG AGT ATT GCG GGG GAA GGT
G10T-A23G-29	CGC ACC TGG TGG AGT ATT GCG GGG GAA GG
G10T-A23G-29-MB	/Thiol-C6/-CCT GGT GGA GTA TTG CGG GGG AAG G-/MB/
A23T-29-MB	/Thiol-C6/-CGC TCC TGG GGG AGT ATT GCG GTG GAAG GTT T-/MB/
A10-excised	GTA TTG CGG AGG AAG GTT TTT AAC CTT CGG GG
Tasset	AGT CCG TGG TAG GGC AGG TTG GGG TGA CT
Bock	GGT TGG TGT GGT TGG
Bock-hang	TAA GTT CAT CTC CCC GGT TGG TGT GGT TGG
IgE Aptamer	GGG GCA CGT TTA TCC GTC CCT CCT AGT GGC GTG CCC C

a. Mutated nucleotides are colored red and underlined

b. /Thiol-C6/ represents a 5' modified thiol group with a six-carbon spacer

c. /MB/ represents a 3' modified methylene blue redox reporter

Table S2. Ochratoxin-binding aptamers, ligands, and aptamer/ligand concentration used for ITC and determined K_D.

Aptamer	Ligand	[Ligand] (μM)	[Aptamer] (μM)	K_D (μM)
OBA1	OTA	15	250	5.5 ± 0.2
OBA1	OTB	15	500	74.1 ± 9.5
OBA3	OTA	15	250	1.8 ± 0.1
OBA3	OTB	15	500	25.5 ± 1.2
OBA5	OTA	15	250	3.4 ± 0.1
OBA5	OTB	15	500	59.9 ± 6.9
Tasset	Thrombin	5	50	0.0136 ± 0.0031
Bock	Thrombin	5	50	0.0231 ± 0.0054
Bock-hang	Thrombin	7.5	75	0.097 ± 0.019

Table S3. ATP-binding aptamers, ligands, and ligand concentration used for ITC and determined K_{D1}, K_{D2}, and $K_{1/2}$.

Aptamer	Ligand	[Ligand] (μM)	Injection volume (μL)	K_{D1} (μM)	K_{D2} (μM)	$K_{1/2}$ (μM)
ATPwt	ADE	800	1	1.3 ± 0.1	13.7 ± 0.3	4.2 ± 0.1
ATPwt	AMP	800	1	6.4 ± 0.1	30.9 ± 0.4	14.1 ± 0.2
ATPwt	ADP	800	1	2.1 ± 0.1	19.1 ± 0.3	6.3 ± 0.1
ATPwt	ATP	800	1	4.4 ± 0.1	23.9 ± 0.4	10.2 ± 0.2
A23T	ADE	1,800	1	7.0 ± 0.5	29.1 ± 0.6	14.3 ± 0.6
A23T-30	ADE	1,800	1	13.1 ± 0.5	26.6 ± 0.6	18.6 ± 1.7
A23T-29	ADE	1,800	1	35.3 ± 1.0	39.8 ± 0.6	37.4 ± 6.2
A23T-29	AMP	1,200	2	NA	NA	>1000
A23T-29	ADP	1,200	2	169.5 ± 3.4	480.8 ± 9.7	285.4 ± 5.7
A23T-29	ATP	1,200	2	327.8 ± 17.2	505.0 ± 28.1	406.3 ± 21.8
G10T-A23G	ADE	1,200	1	7.3 ± 0.2	32.4 ± 0.5	15.3 ± 0.2
G10T-A23G-30	ADE	1,200	1	8.8 ± 0.2	37.1 ± 0.6	18.1 ± 0.4
G10T-A23G-29	ADE	1,200	1	9.2 ± 0.2	37.4 ± 0.6	18.5 ± 0.4
G10T-A23G-29	AMP	1,200	2	352.1 ± 12.4	131.4 ± 4.3	214.7 ± 7.2
G10T-A23G-29	ADP	1,200	2	167.9 ± 3.0	142.6 ± 2.4	162.9 ± 2.8
G10T-A23G-29	ATP	1,200	2	50.2 ± 1.4	591.7 ± 13.6	171.9 ± 4.3
A23G	ADE	1,500	1	6.7 ± 0.4	28.3 ± 0.9	13.8 ± 0.6
A23C	ADE	1,500	1	1.5 ± 0.1	17.1 ± 0.5	5.0 ± 0.3
A26T	ADE	1,000	1	8.6 ± 0.6	1297 ± 153	105.6 ± 9.5
A26G	ADE	1,000	1	5.5 ± 0.6	3246 ± 1897	133.6 ± 33.0
A10-excised	ADE	1,000	2	311.5 ± 11.3	NA	NA

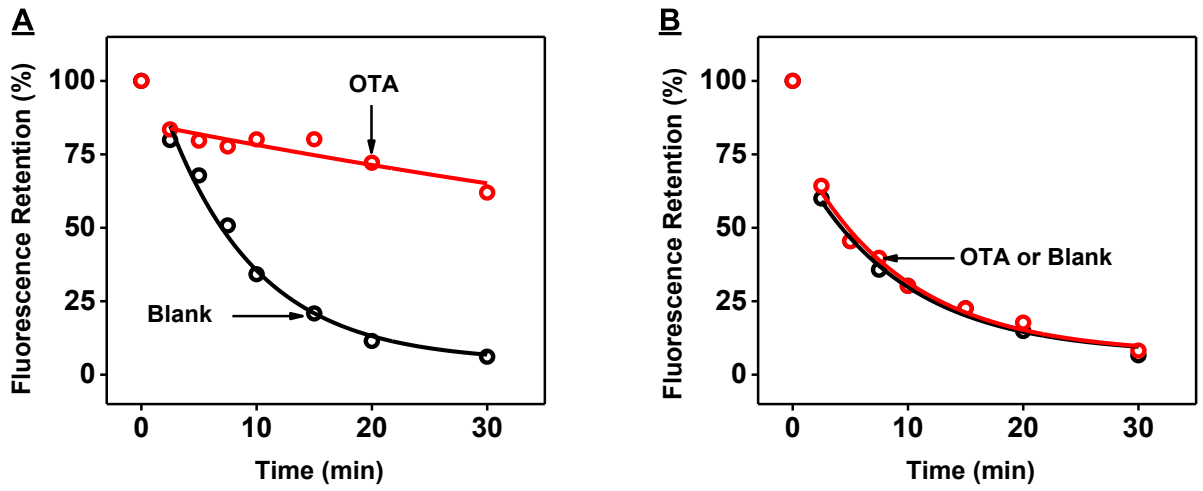

Figure S1. Fluorescence time-course of the digestion of (**A**) OBA3 and (**B**) OBA4 with the mixture of Exo III and Exo I in the absence (black) and presence of 100 μM OTA (red).

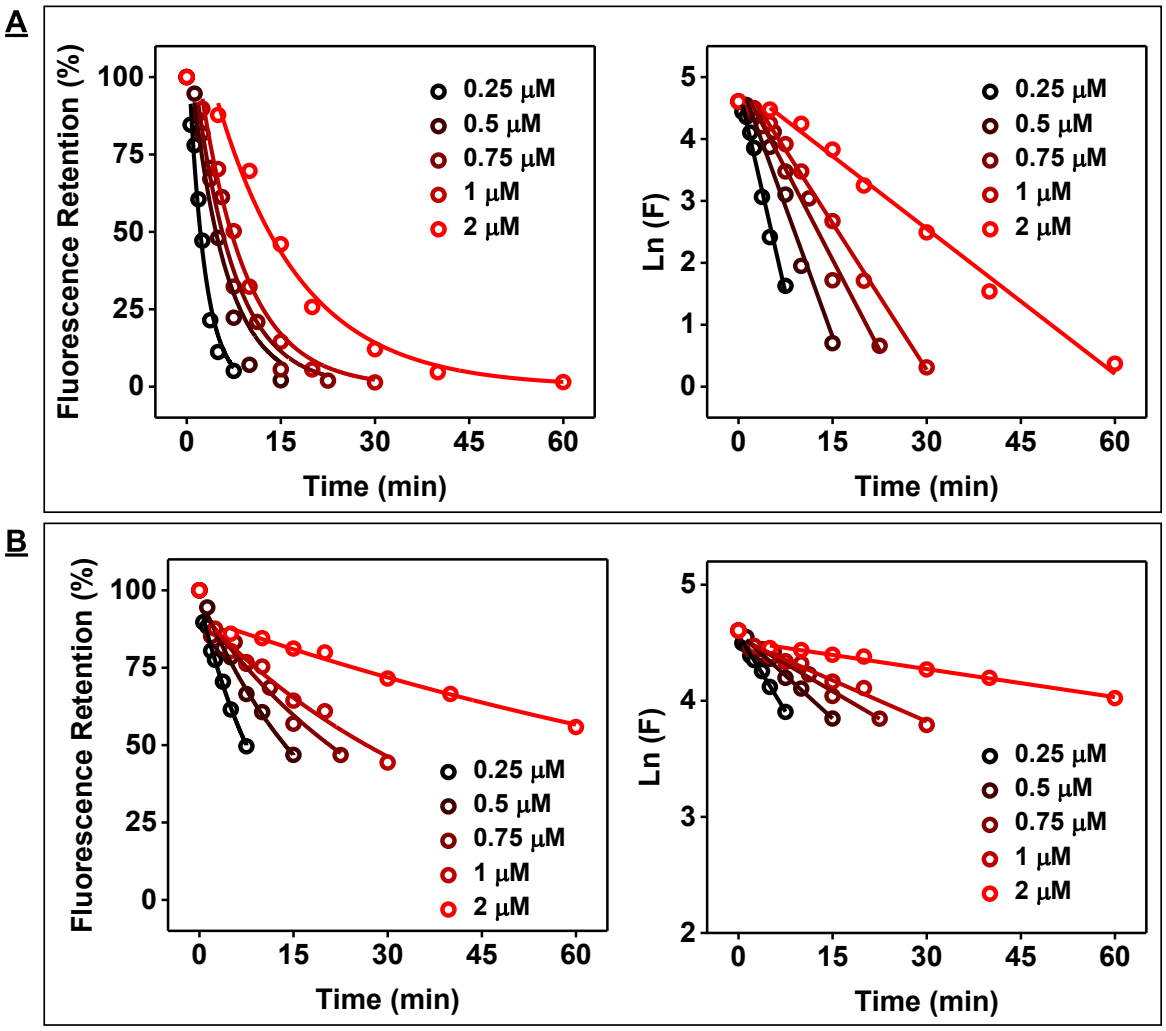

Figure S2. Characterization of OBA3 digestion kinetics by Exo III and Exo I. Fluorescence time-course of the digestion (left) of 0.25, 0.5, 0.75, 1, or 2 μM OBA3 (indicated by black to red color gradient) and natural log plot (right) of fluorescence retention in the (**A**) absence and (**B**) presence of 25 μM OTA.

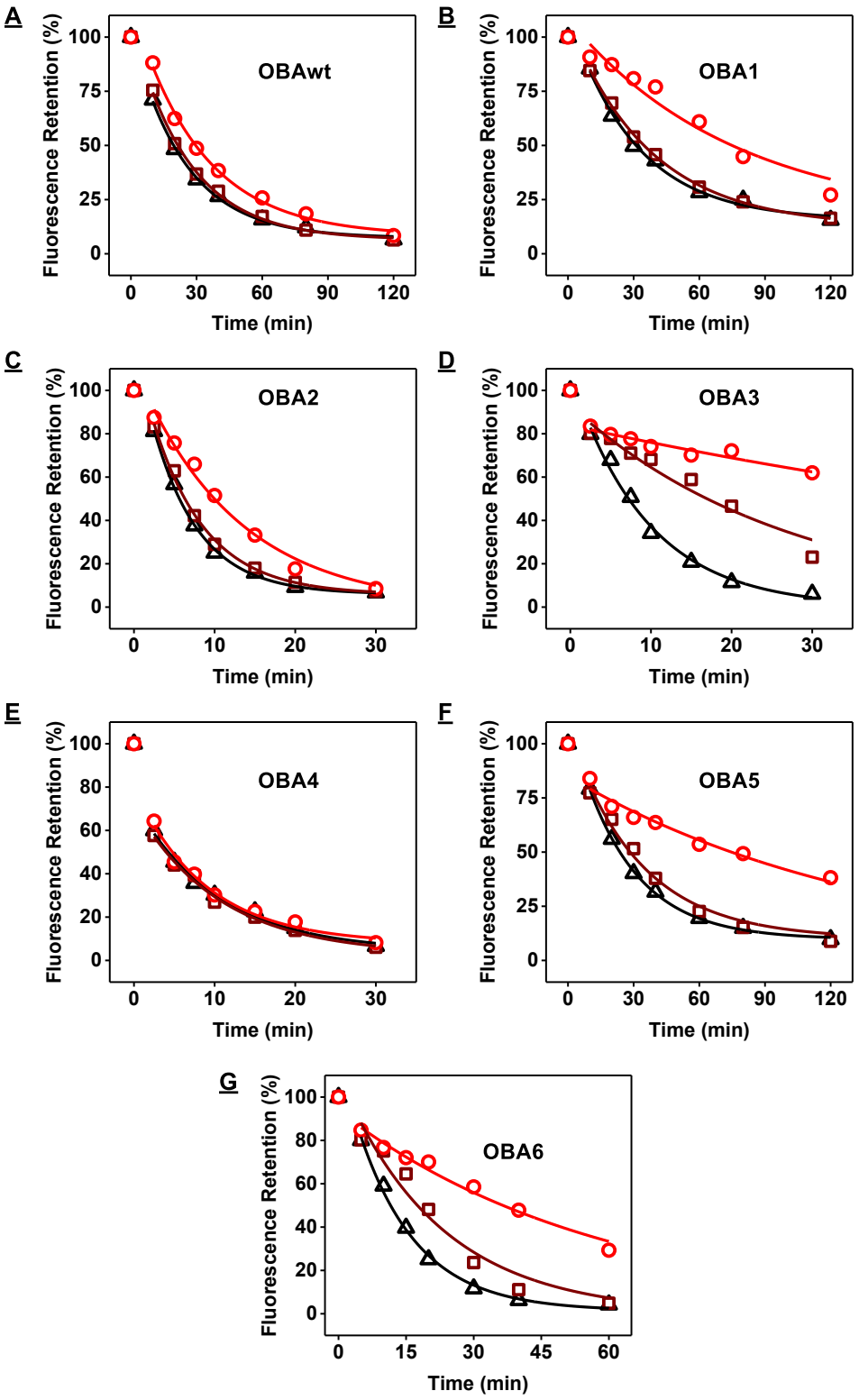

Figure S3. Evaluation of the binding profile of OTA-binding aptamers using the exonuclease digestion assay. Digestion of (**A**) OBAwt, (**B**) OBA1, (**C**) OBA2, (**D**) OBA3, (**E**) OBA4, (**F**) OBA5, and (**G**) OBA6 with the mixture of Exo III and Exo I in the absence (black triangles) or presence of 100 μM OTA (red circles) or 100 μM ochratoxin B (OTB) (burgundy squares).

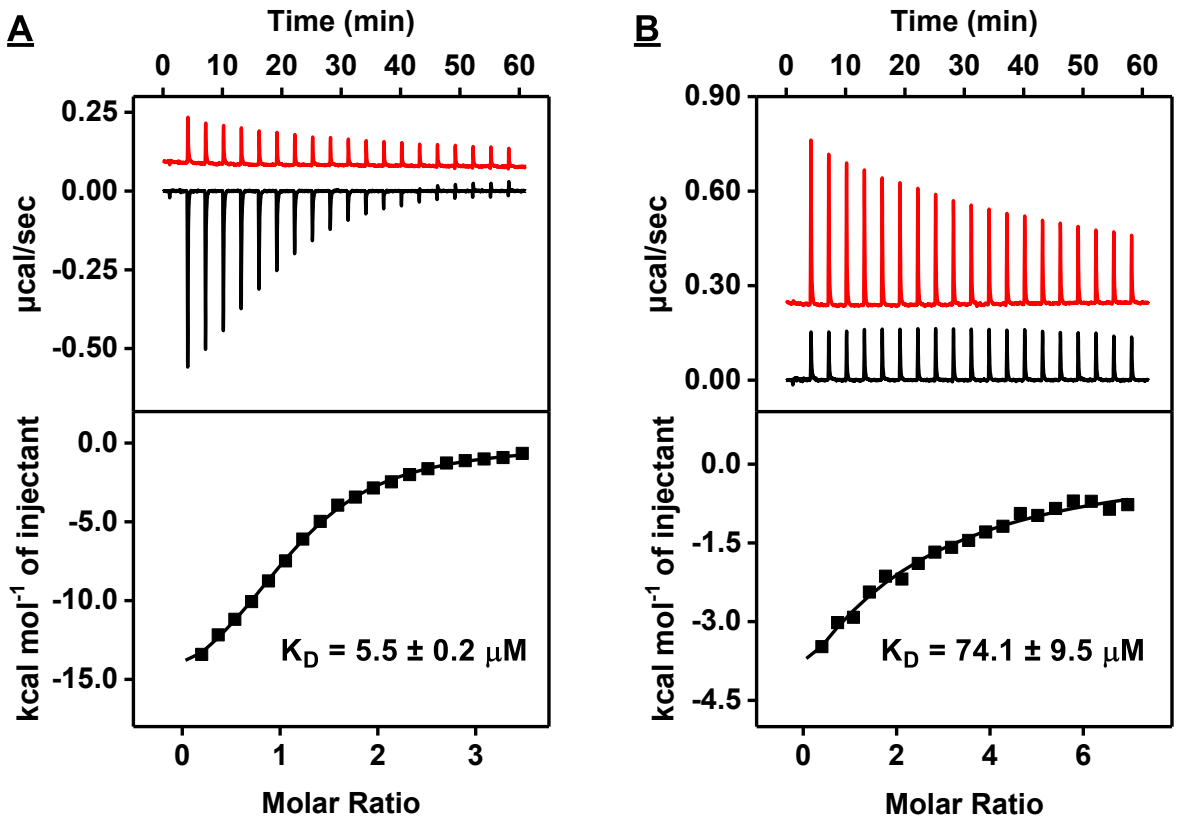

Figure S4. Characterization of OBA1 affinity for OTA and OTB using isothermal titration calorimetry (ITC). Top panels display the heat generated from each titration of OBA1 to (**A**) buffer (red) or OTA (black) and (**B**) buffer (red) or OTB (black). Bottom panels show the integrated heat of each titration after correcting for the heat of dilution of the titrant.

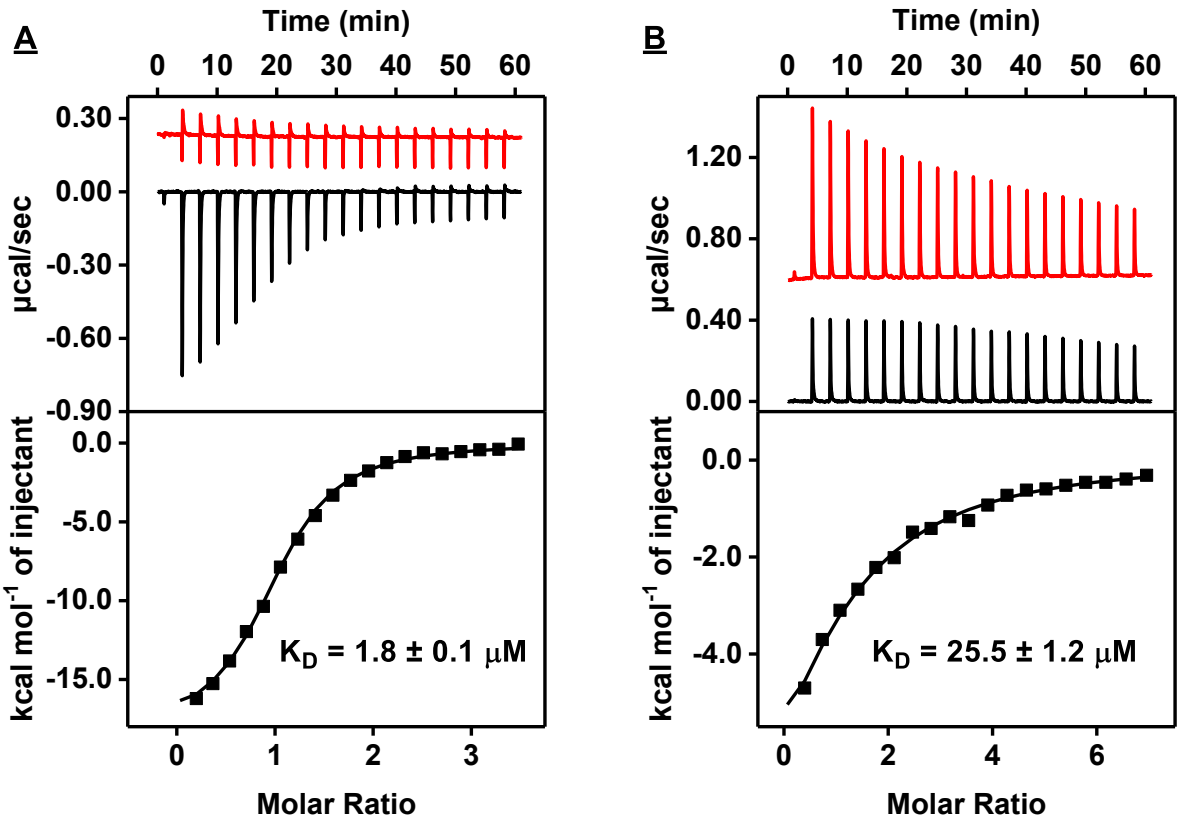

Figure S5. Characterization of OBA3 affinity for OTA and OTB using ITC. Top panels display the heat generated from each titration of OBA3 to (**A**) buffer (red) or OTA (black) and (**B**) buffer (red) or OTB (black). Bottom panels show the integrated heat of each titration after correcting for the heat of dilution of the titrant.

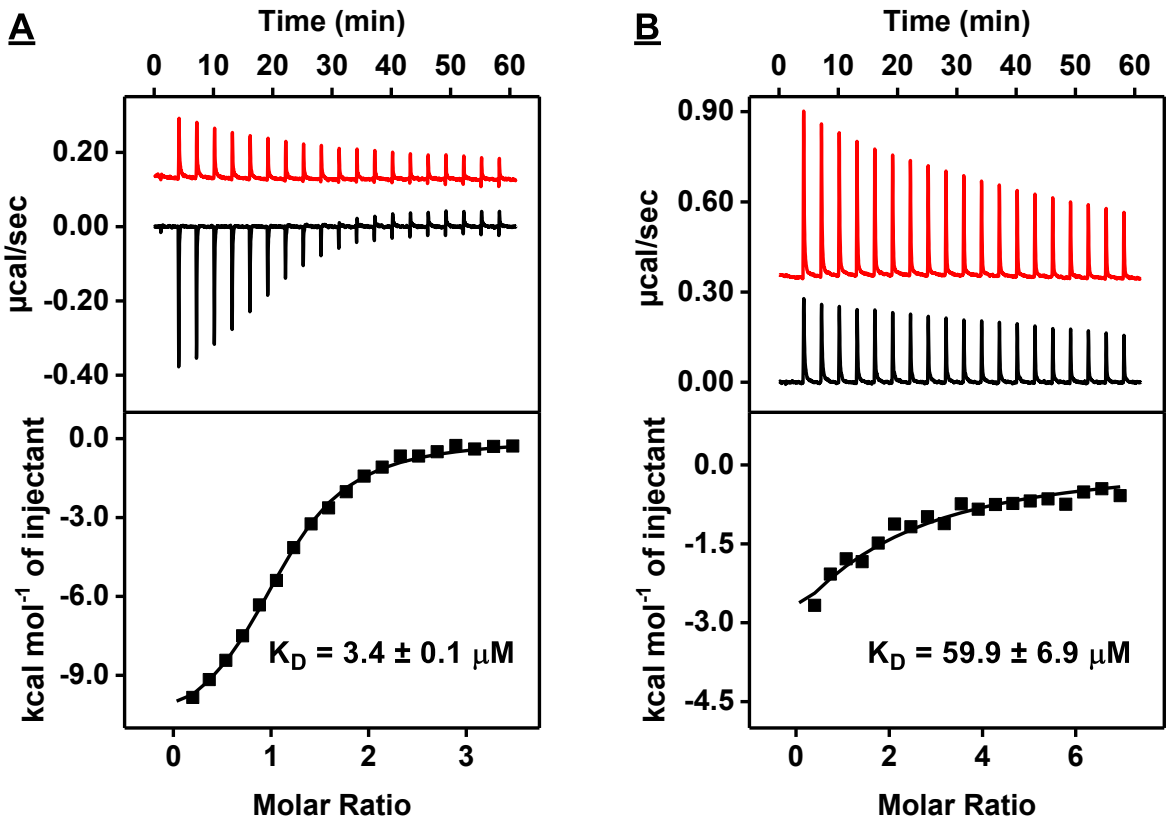

Figure S6. Characterization of OBA5 affinity for OTA and OTB using ITC. Top panels display the heat generated from each titration of OBA5 to (**A**) buffer (red) or OTA (black) and (**B**) buffer (red) or OTB (black). Bottom panels show the integrated heat of each titration after correcting for the heat of dilution of the titrant.

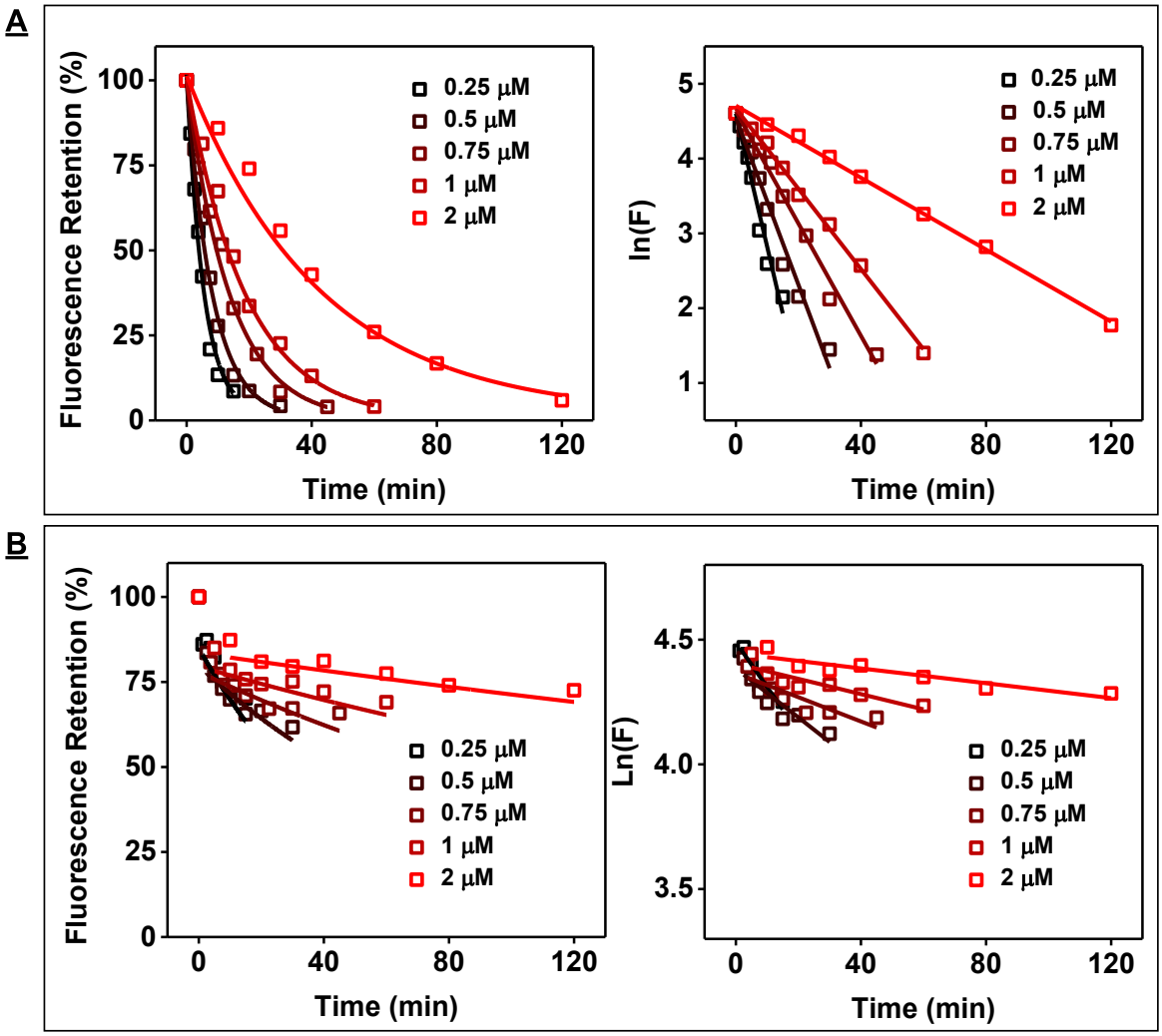

Figure S7. Characterization of ATPwt digestion kinetics by Exo III and Exo I. Time-course digestion (left) of 0.25, 0.5, 0.75, 1, or 2 μM ATPwt (indicated by the black to red color gradient) and natural log plot (right) of digestion progress (**A**) in the absence and (**B**) presence of 250 μM ATP.

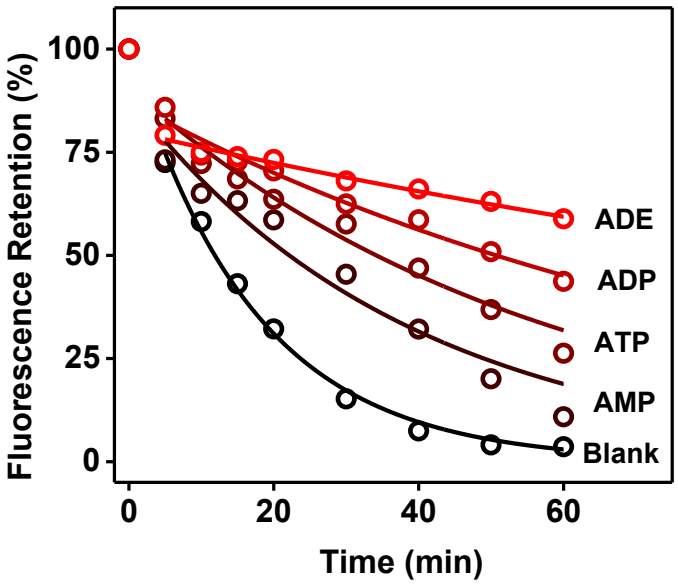

Figure S8. Digestion of ATPwt with Exo III and Exo I in the absence and presence of 100 μM ADE, AMP, ADP, or ATP.

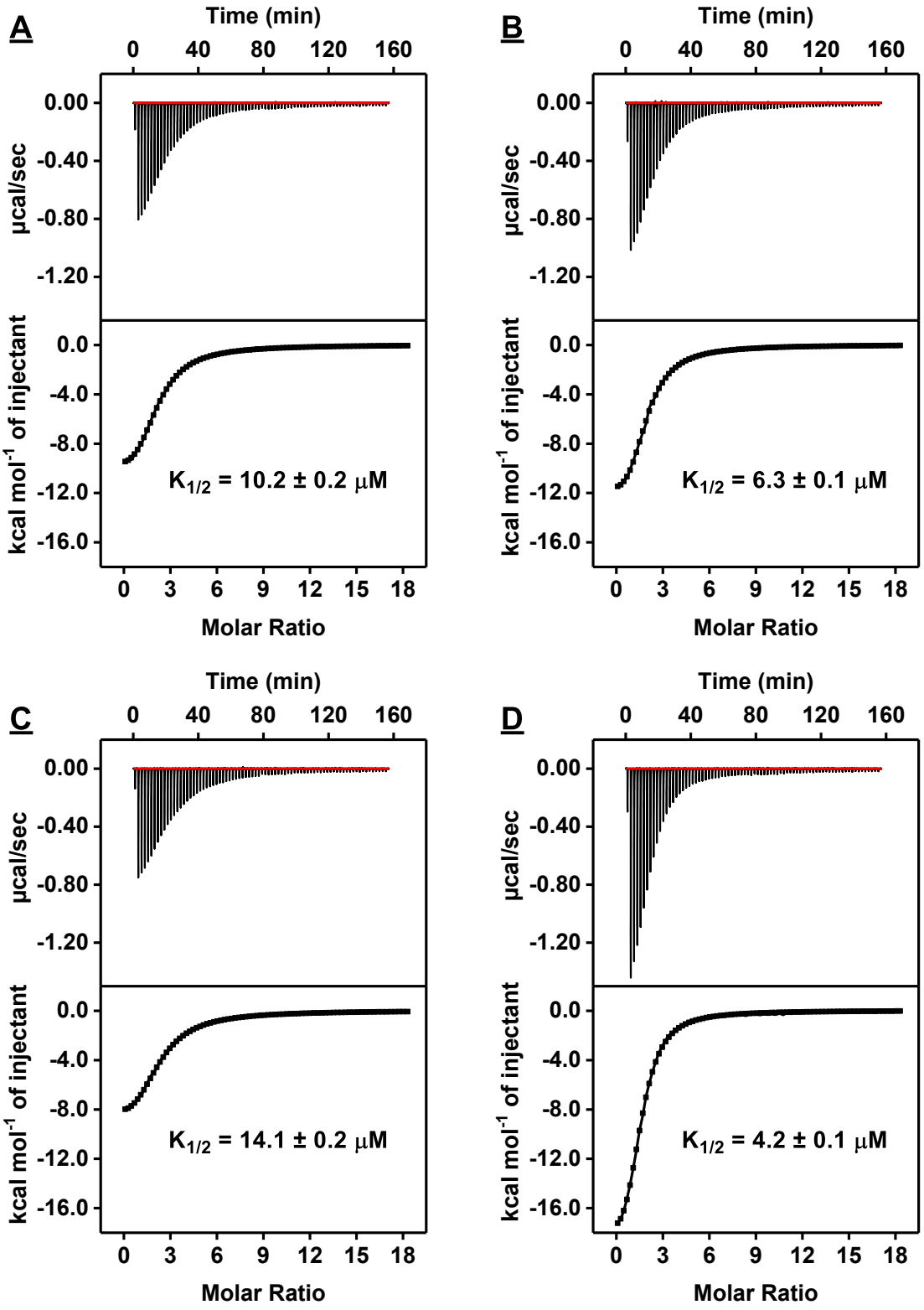

Figure S9. Characterization of affinity of ATPwt to ATP, ADP, AMP, and ADE using ITC. Top panels display the heat generated from each titration of (**A**) ATP, (**B**) ADP, (**C**) AMP, and (**D**) ADE to ATPwt. Bottom panels show the integrated heat of each titration after correcting for the heat of dilution of the titrant.

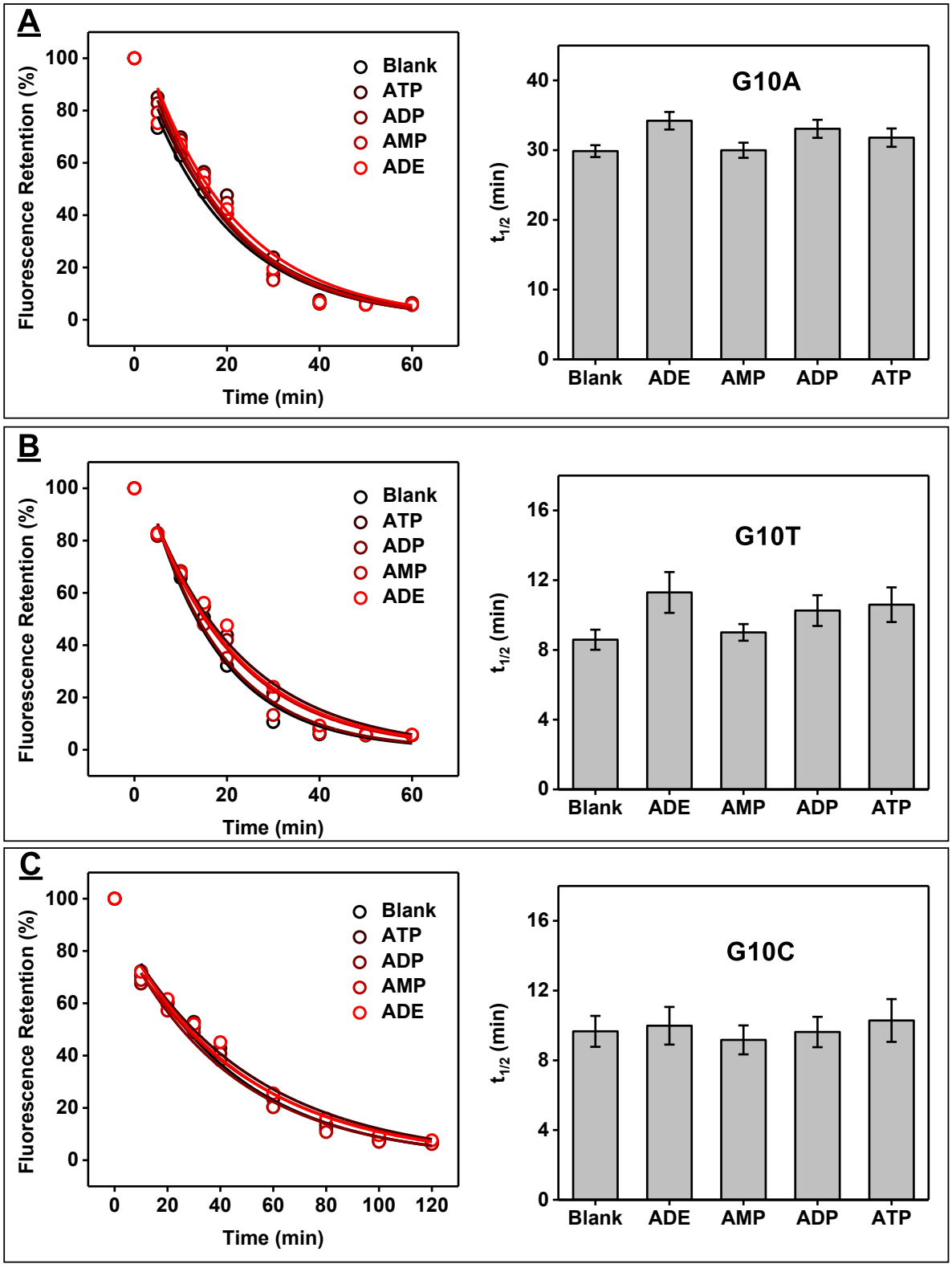

Figure S10. Evaluating the binding profile of various G10 mutant aptamers using the exonuclease digestion assay. Fluorescence time-course for the digestion (left) and calculated $t_{1/2}$ (right) of (**A**) G10A, (**B**) G10T, and (**C**) G10C in the absence or presence of 250 μM ATP, ADP, AMP, or ADE.

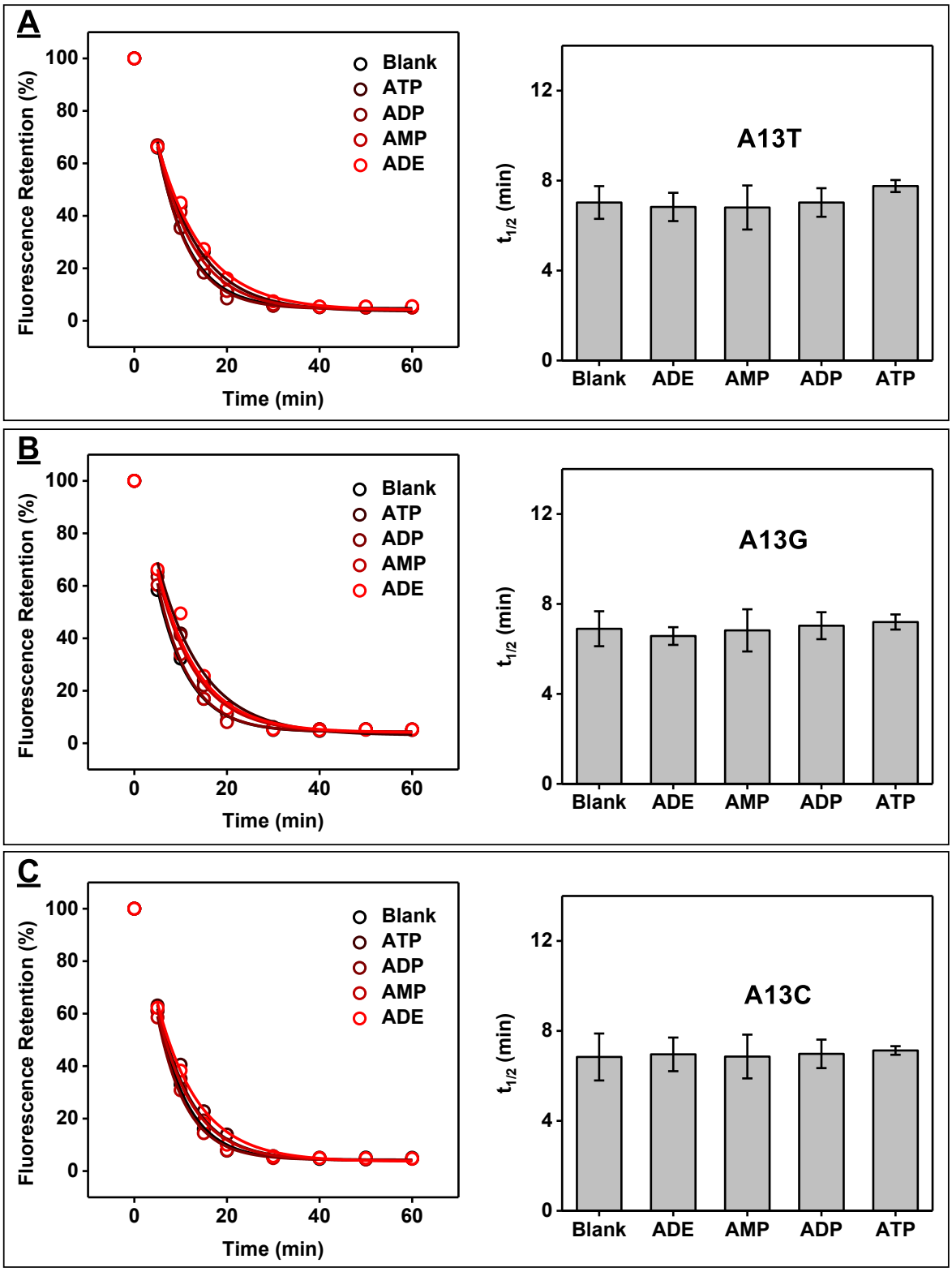

Figure S11. Evaluating the binding profile of various A13 mutant aptamers using the exonuclease digestion assay. Fluorescence time-course for the digestion (left) and calculated $t_{1/2}$ (right) of (**A**) A13T, (**B**) A13G, and (**C**) A13C in the absence or presence of 250 µM ATP, ADP, AMP, or ADE.

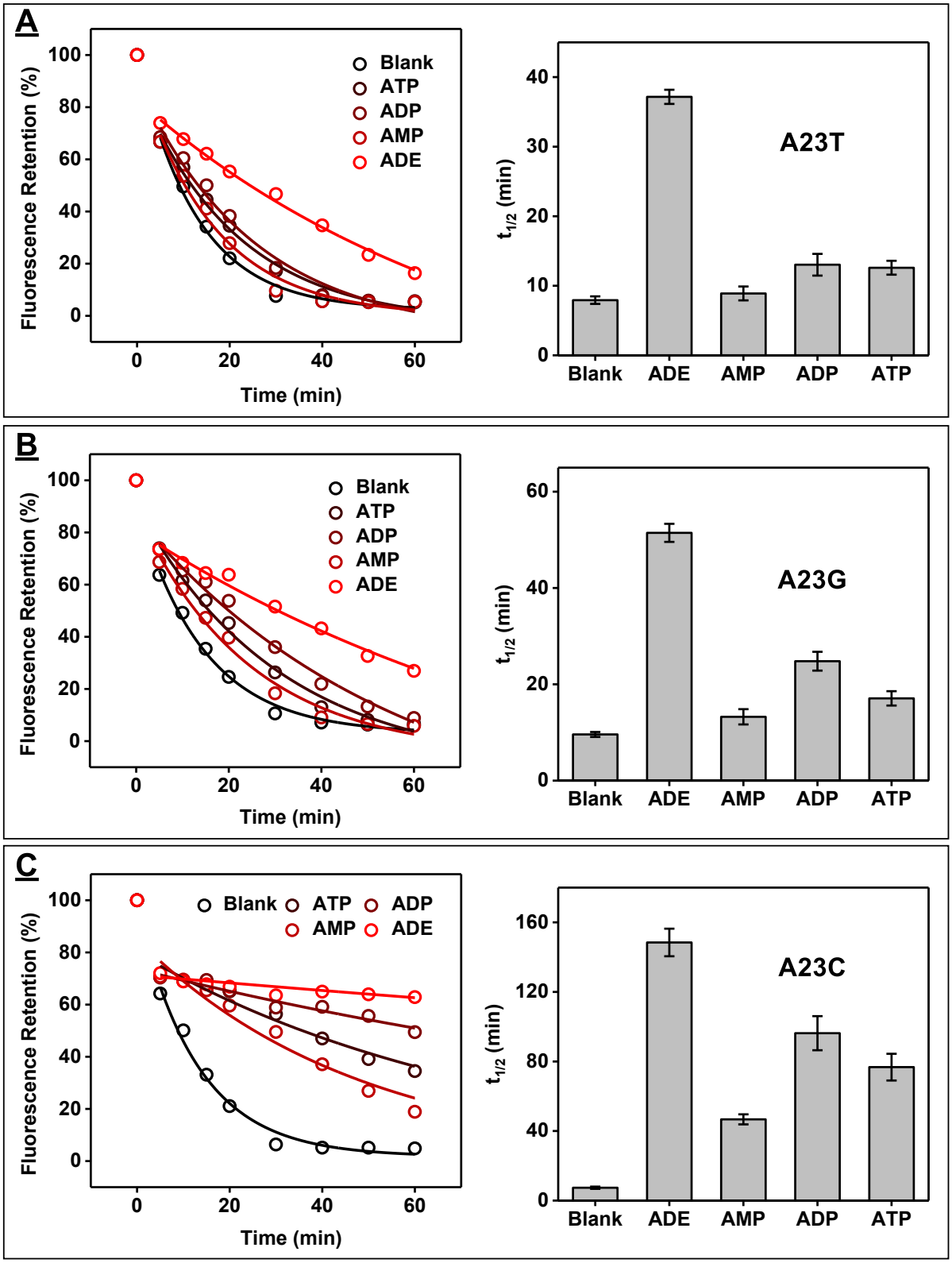

Figure S12. Evaluating the binding profile of various A23 mutant aptamers using the exonuclease digestion assay. Fluorescence time-course for the digestion (left) and calculated $t_{1/2}$ (right) of (**A**) A23T, (**B**) A23G, and (**C**) A23C in the absence or presence of 250 µM ATP, ADP, AMP, or ADE.

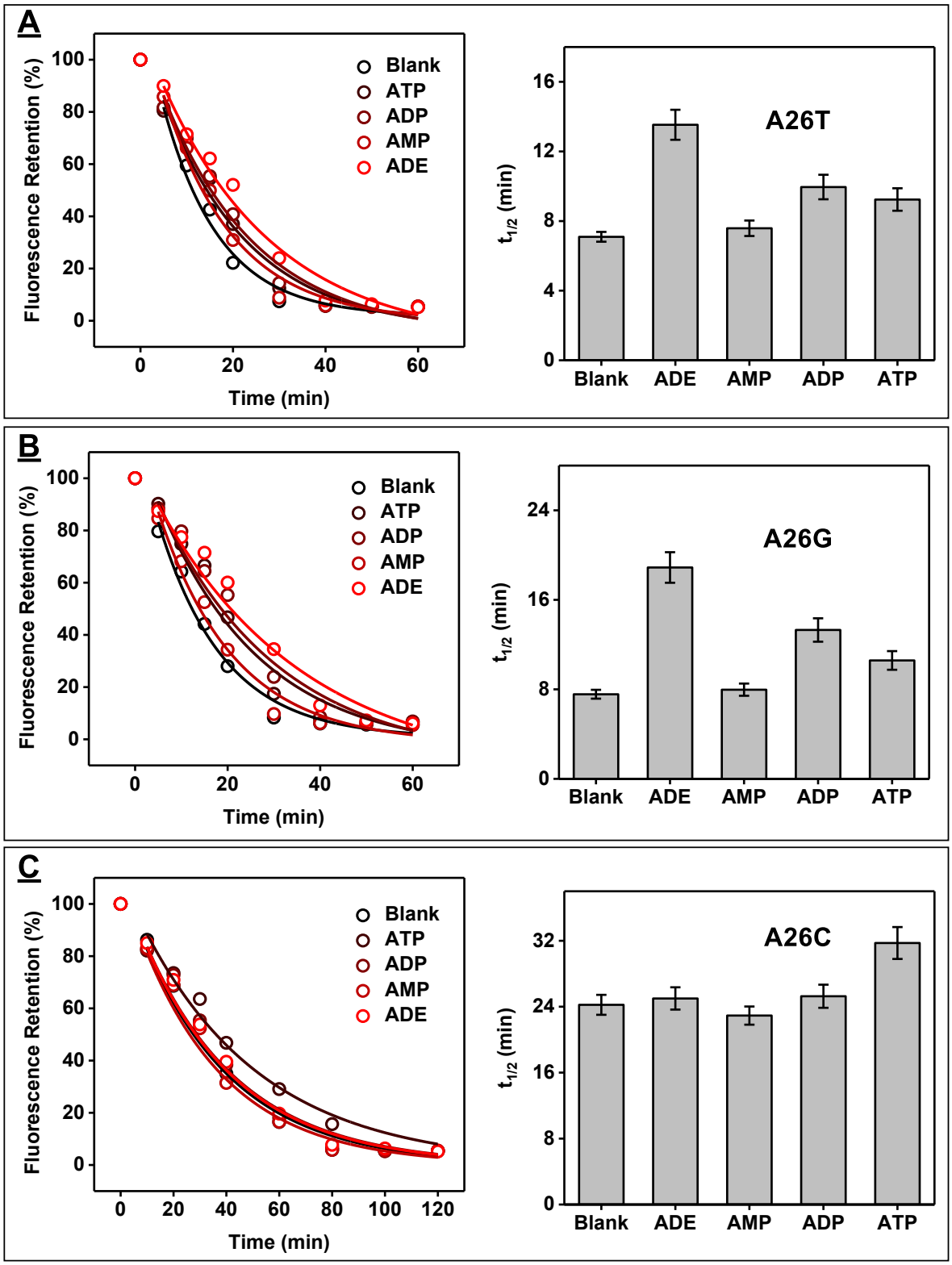

Figure S13. Evaluating the binding profile of various A26 mutant aptamers using the exonuclease digestion assay. Fluorescence time-course for the digestion (left) and calculated $t_{1/2}$ (right) of (**A**) A26T, (**B**) A26G, and (**C**) A26C in the absence or presence of 250 µM ATP, ADP, AMP, or ADE.

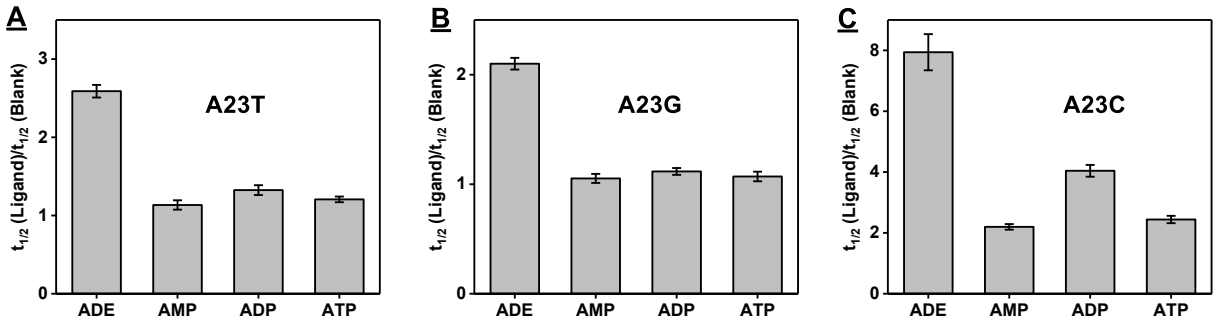

Figure S14. Binding profile of A23 mutants determined using the exonuclease digestion assay. $t_{1/2}$ ratio of (**A**) A23T, (**B**) A23G, and (**C**) A23C in the presence of 100 μM ATP, ADP, AMP, or ADE.

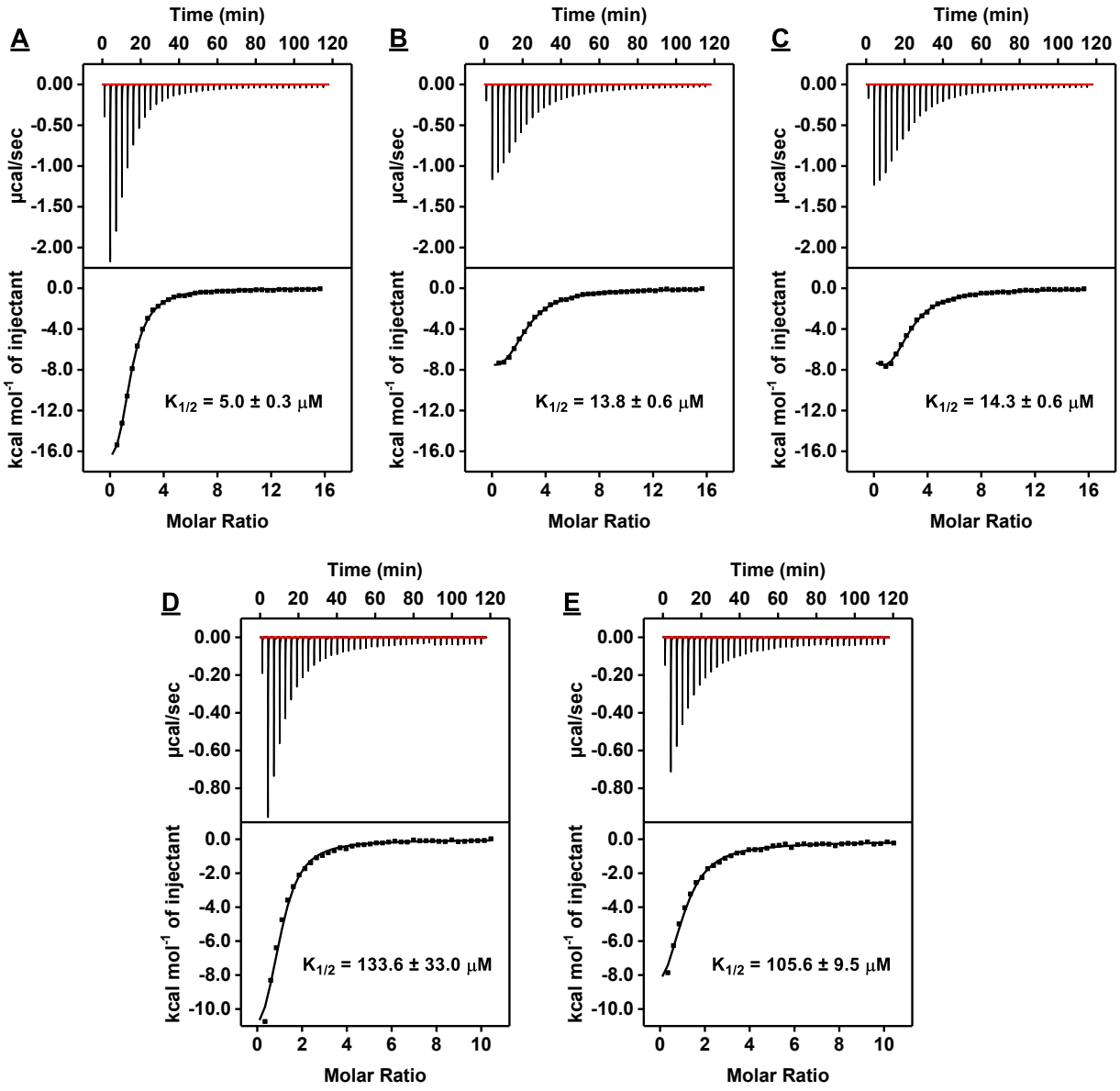

Figure S15. Characterization of affinity of single-site mutants for ADE using ITC. Top panels display the heat generated from each titration of ADE to (**A**) A23C, (**B**) A23G, (**C**) A23T, (**D**) A26G, and (**E**) A26T. Bottom panels show the integrated heat of each titration after correcting for the heat of dilution of the titrant.

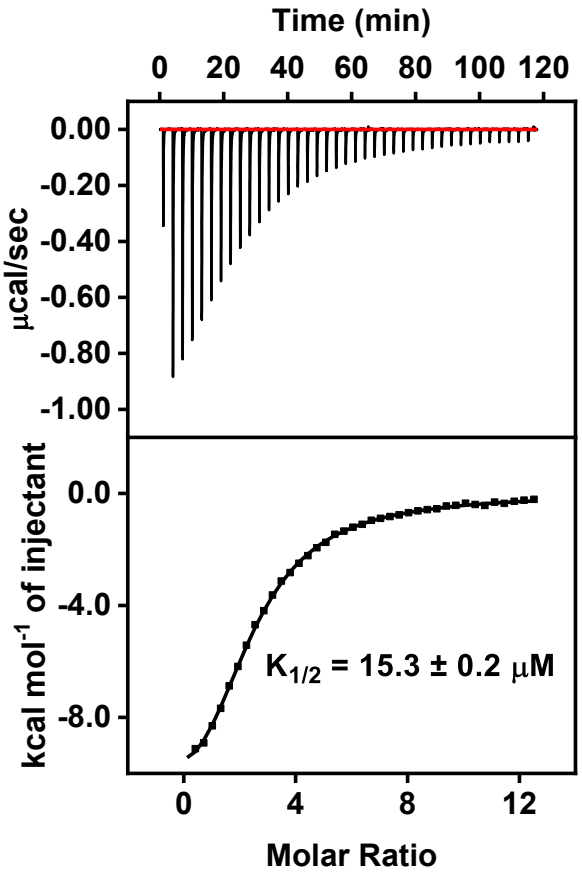

Figure S16. Characterization of affinity of G10T-A23G for ADE using ITC. Top panel displays the heat generated from each titration of ADE to G10T-A23G. Bottom panel shows the integrated heat of each titration after correcting for the heat of dilution of the titrant.

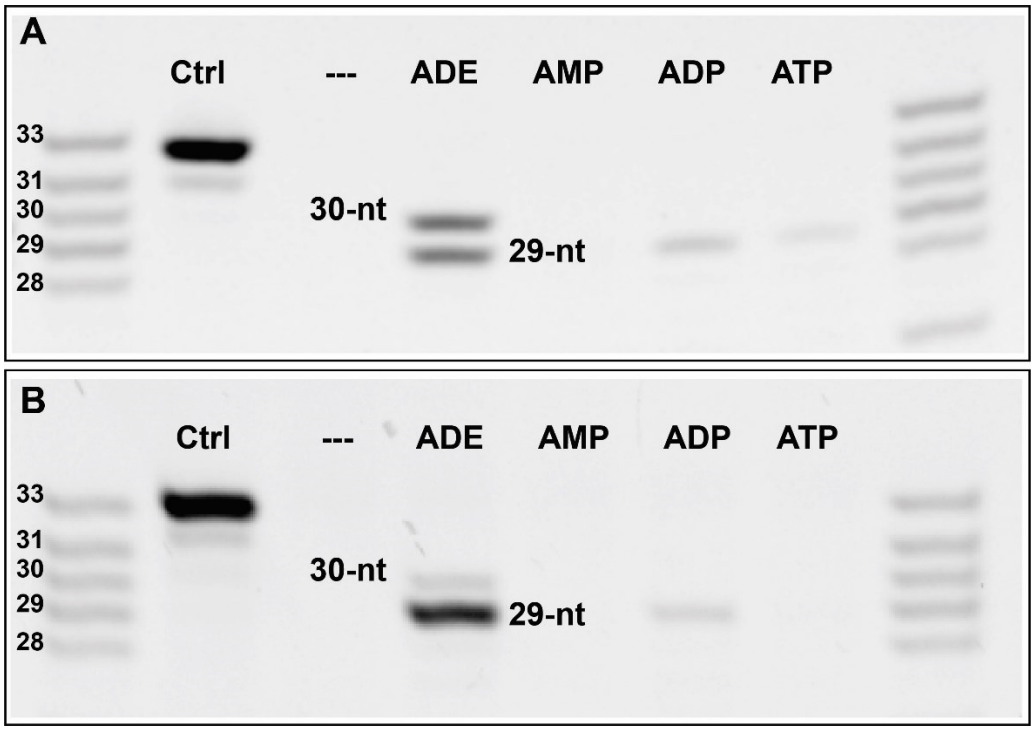

Figure S17. PAGE analysis of (**A**) A23T and (**B**) G10T-A23G products after 30 min of digestion with Exo III and Exo I in the absence or presence of 250 μM ADE, AMP, ADP, or ATP.

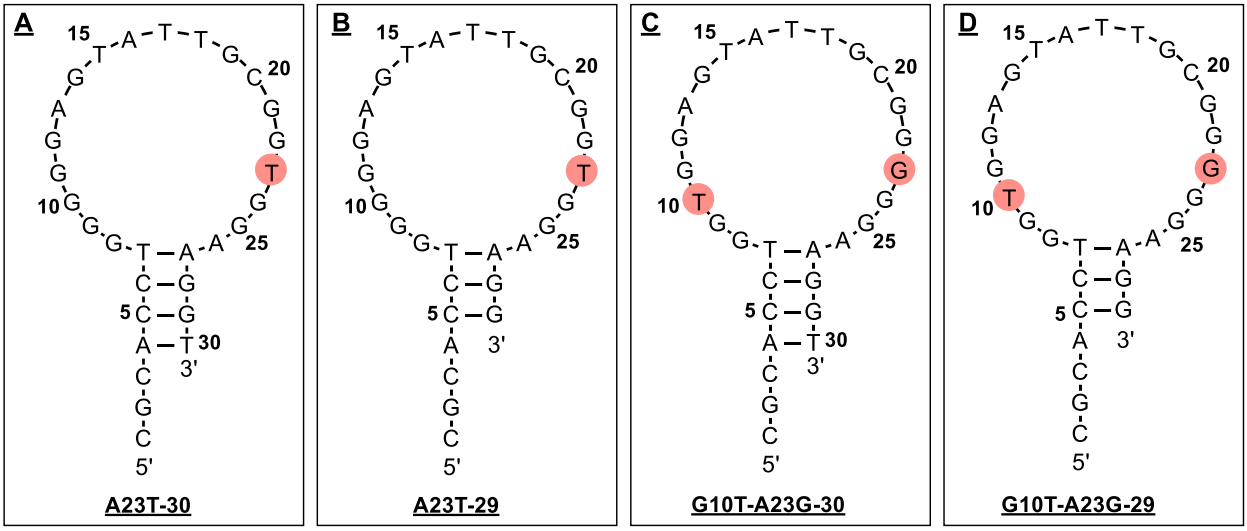

Figure S18. Sequence and secondary structure of (**A**) A23T-30, (**B**) A23T-29, (**C**) G10T-A23G-30, and (**D**) G10T-A23G-29. Mutated nucleotides are marked in red.

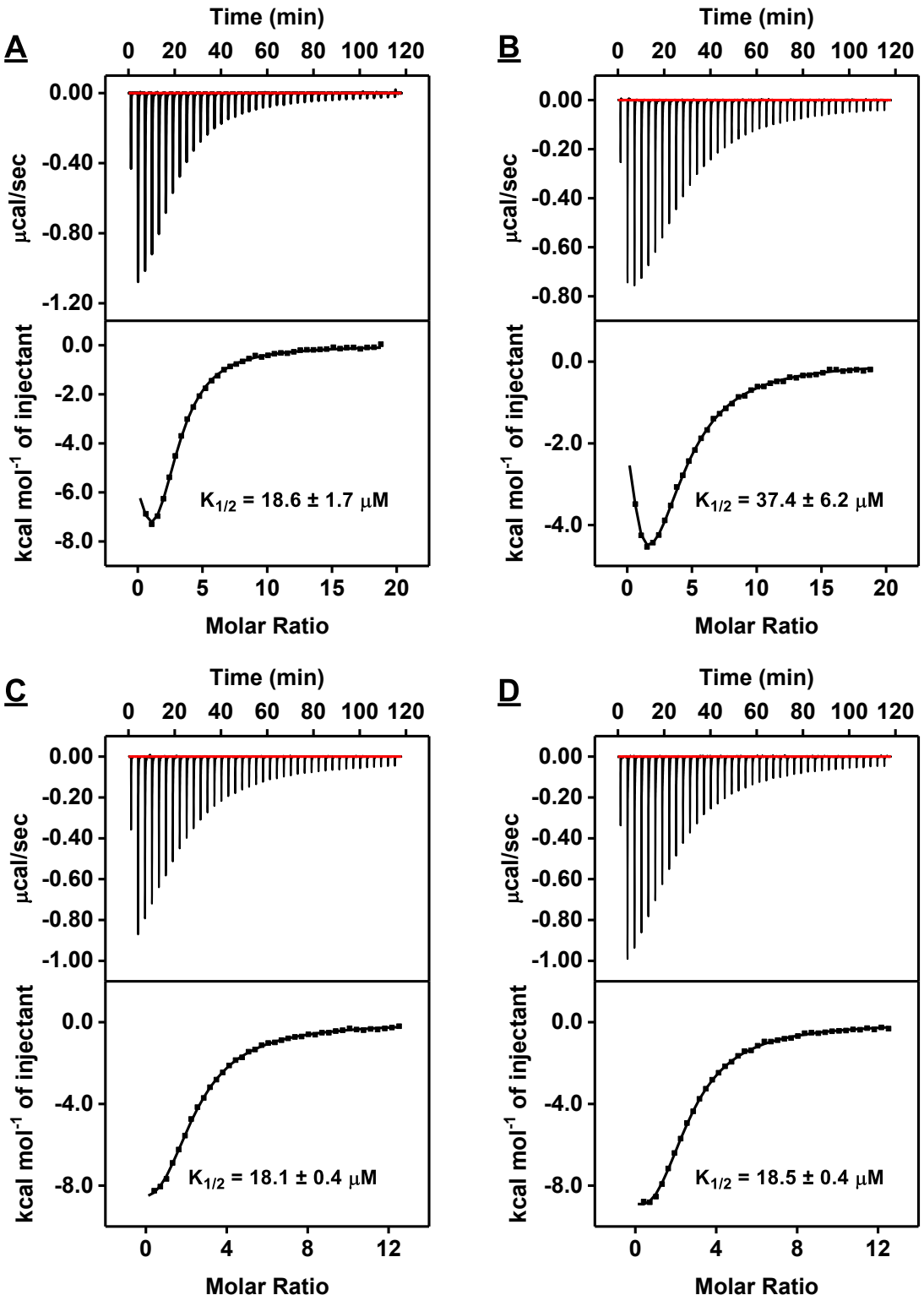

Figure S19. Characterization of affinity of ADE-specific aptamer mutants using ITC. Top panels display the heat generated from each titration of ADE to (**A**) A23T-30, (**B**) A23T-29, (**C**) G10T-A23G-30, and (**D**) G10T-A23G-29. Bottom panels show the integrated heat of each titration after correcting for the heat of dilution of the titrant.

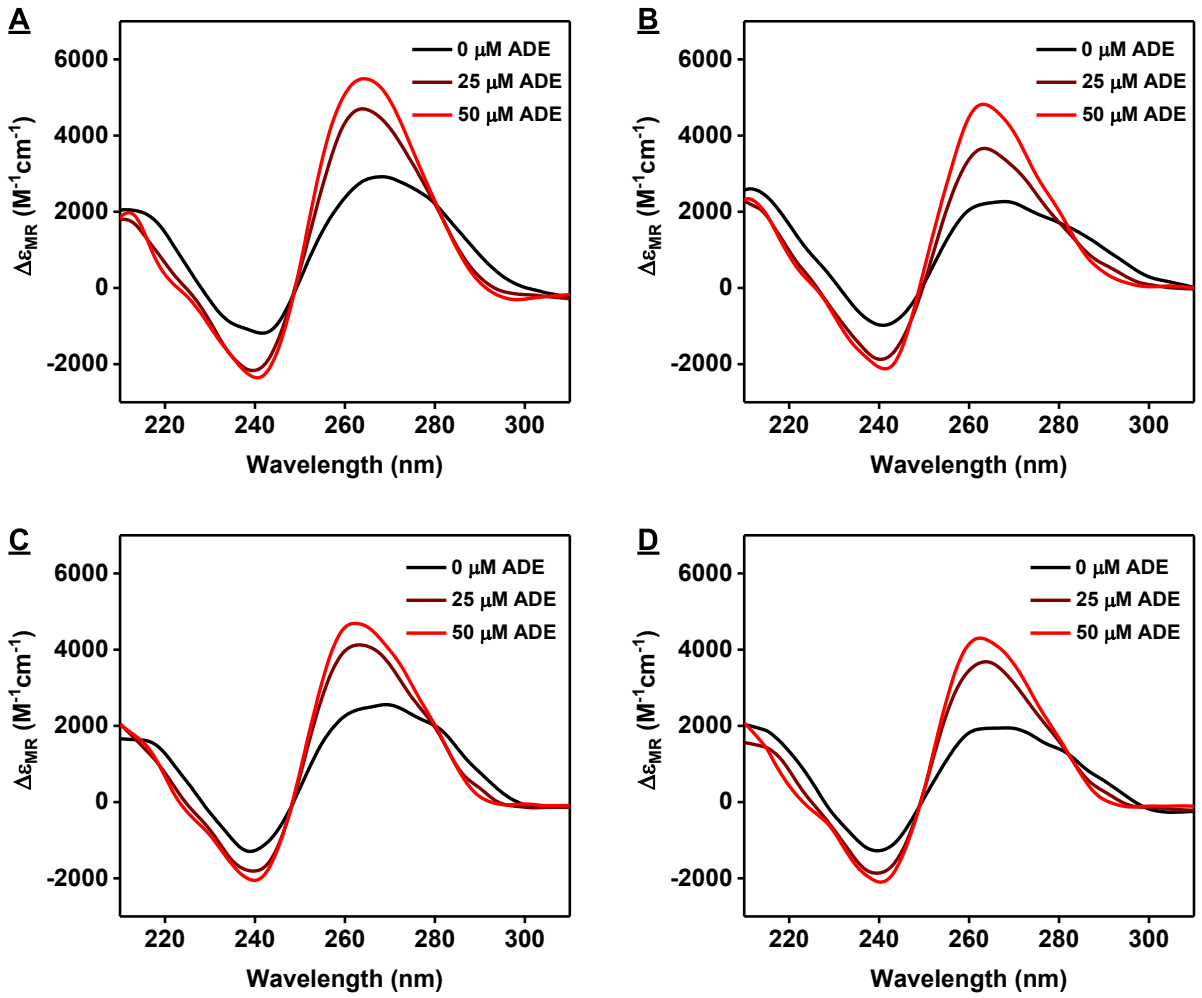

Figure S20. Characterizing structure-switching functionality of A23T and G10T-A23G digestion products using CD spectroscopy. CD spectra of (**A**) A23T-30, (**B**) A23T-29, (**C**) G10T-A23G-30, and (**D**) G10T-A23G-29 in the absence or presence of various concentrations of ADE.

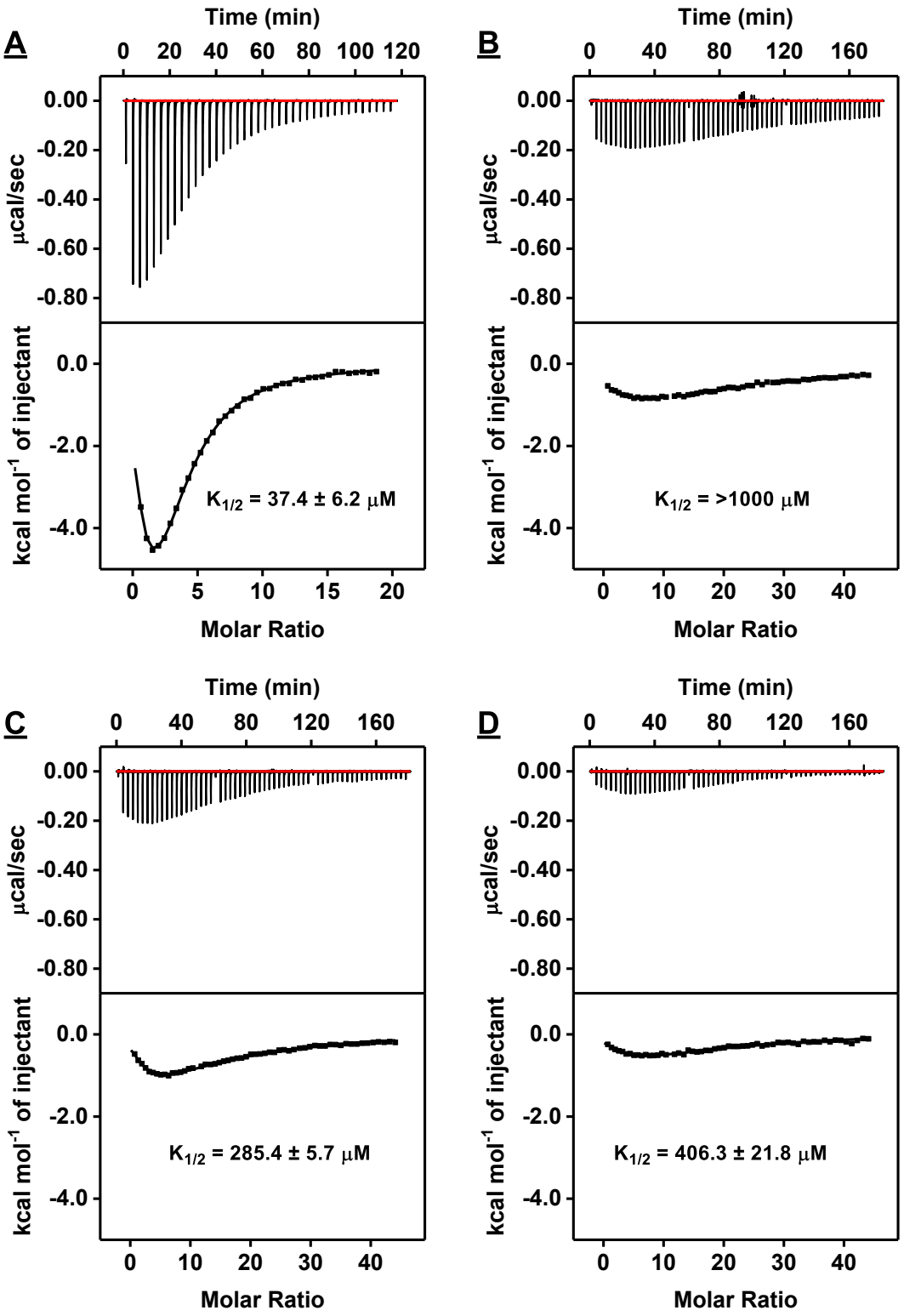

Figure S21. Characterization of A23T-29 affinity using ITC. Top panels display the heat generated from each titration of (**A**) ADE, (**B**) AMP, (**C**) ADP, and (**D**) ATP to A23T-29. Bottom panels show the integrated heat of each titration after correcting for the heat of dilution of the titrant.

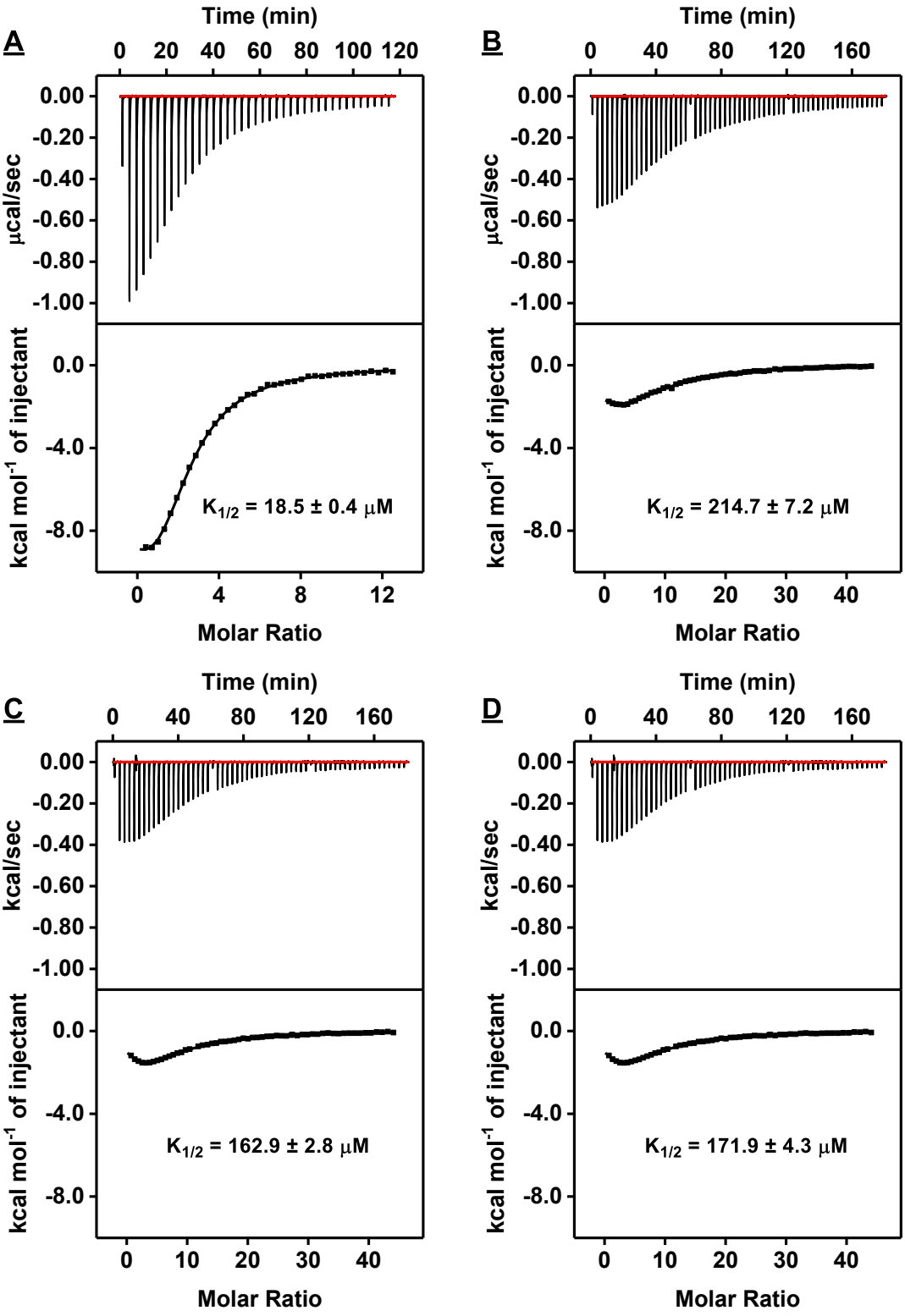

Figure S22. Characterization of G10T-A23G-29 affinity using ITC. Top panels display the heat generated from each titration of (**A**) ADE, (**B**) AMP, (**C**) ADP, and (**D**) ATP to G10T-A23G-29. Bottom panels show the integrated heat of each titration after correcting for the heat of dilution of the titrant.

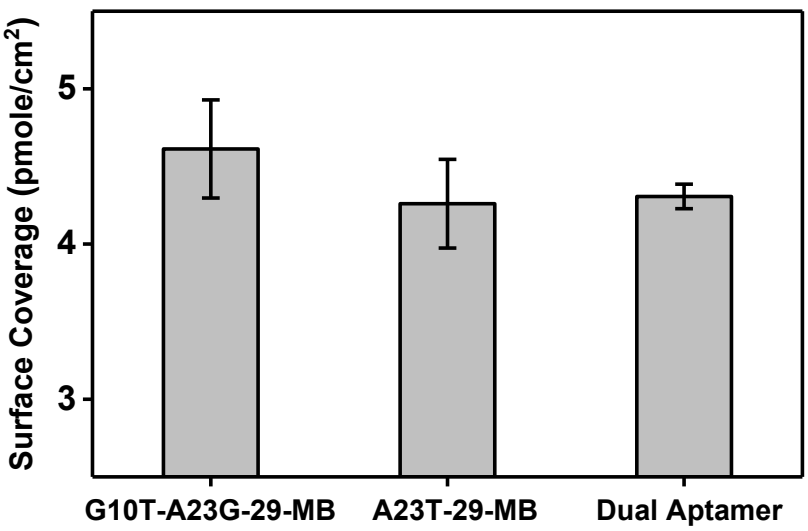

Figure S23. Surface coverage of E-AB sensors fabricated using G10T-A23G-29-MB, A23T-29-MB, or both. The average DNA length was used when calculating the surface coverage of sensors fabricated using both aptamers. Error bars represent the standard deviation of the measurements of three different electrodes.

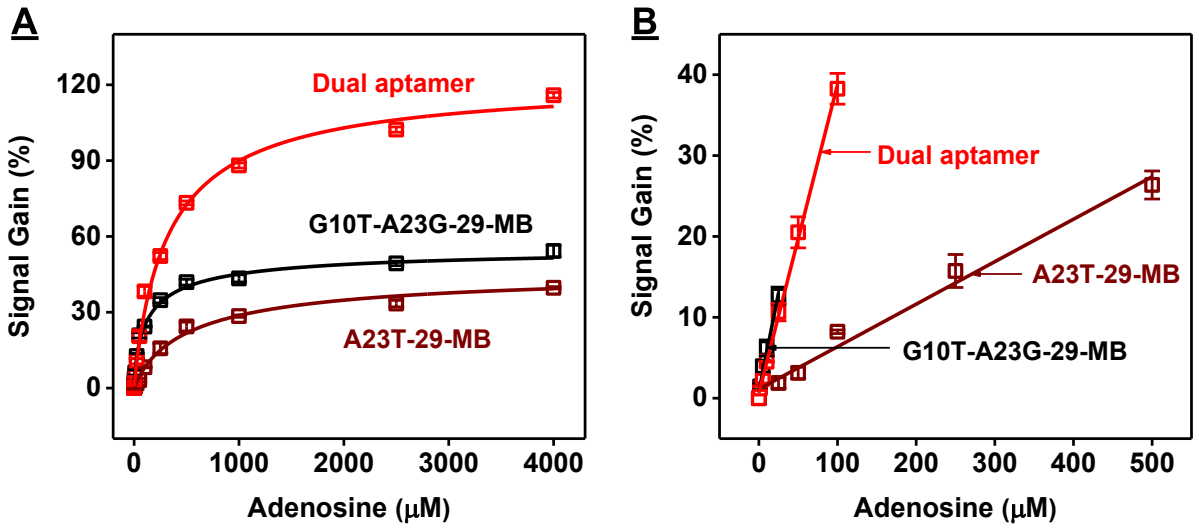

Figure S24. Performance of E-AB sensors fabricated using G10T-A23G-29-MB, A23T-29-MB, or a mixture of both aptamers. (**A**) Calibration curve and (**B**) linear range of the three sensors for the detection of various concentrations of ADE in buffer. Error bars represent the average standard deviation of three electrodes.

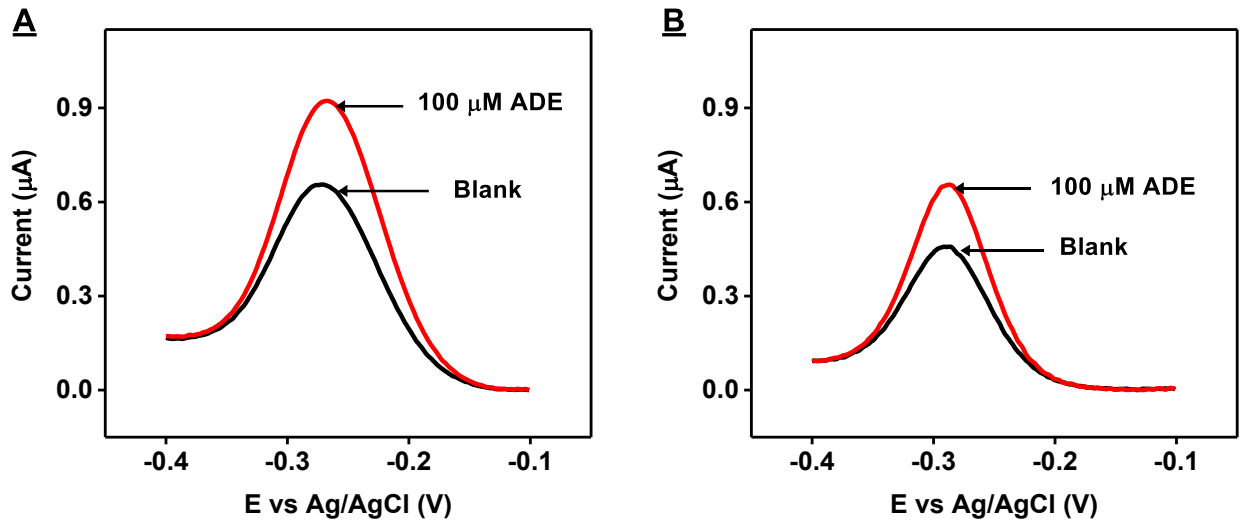

Figure S25. SWV curves in the absence (black) or presence (red) of 100 μM ADE in (**A**) buffer or (**B**) 50% serum using dual-aptamer E-AB sensors constructed with A23T-29-MB and G10T-A23G-29-MB.

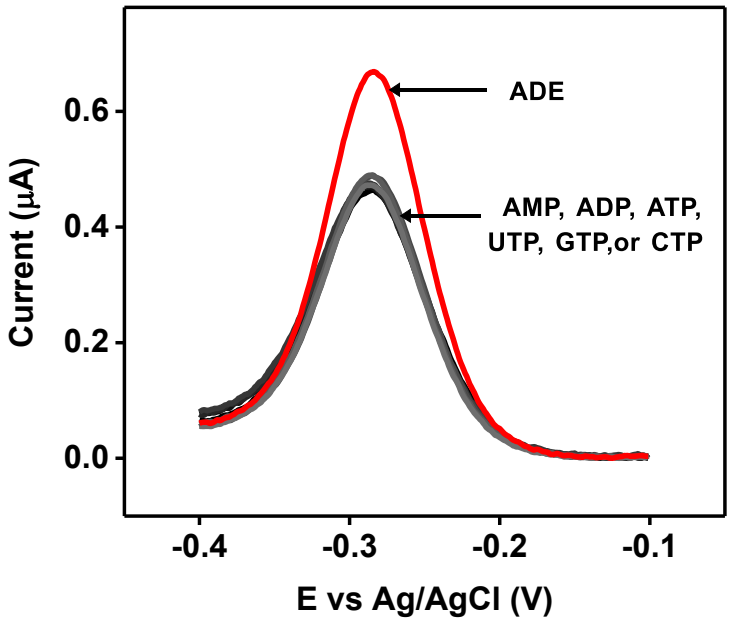

Figure S26. Dual-aptamer E-AB sensor response to 100 μM ADE, AMP, ADP, or ATP or other nucleotide triphosphates in 50% serum.

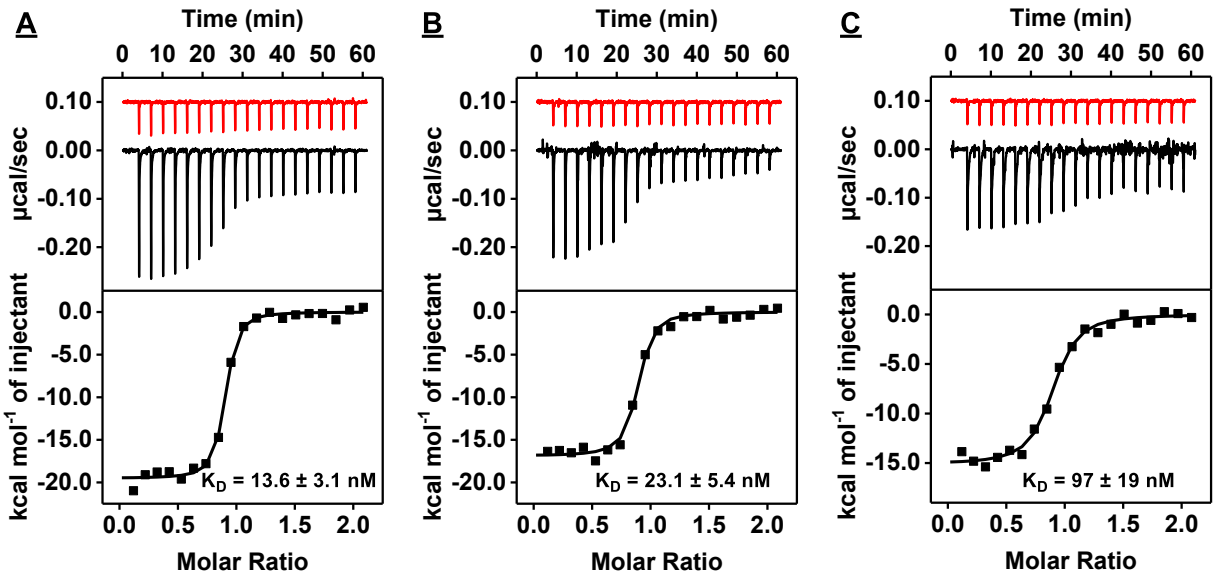

Figure S27. Characterization of the thrombin-binding affinity of Tasset, Bock, and Bock-hang using isothermal titration calorimetry (ITC). Top panels display the heat generated from each titration of (**A**) Tasset, (**B**) Bock and (**C**) Bock-hang to buffer (red) or thrombin (black). Bottom panels show the integrated heat of each titration after correcting for the heat of dilution of the titrant.

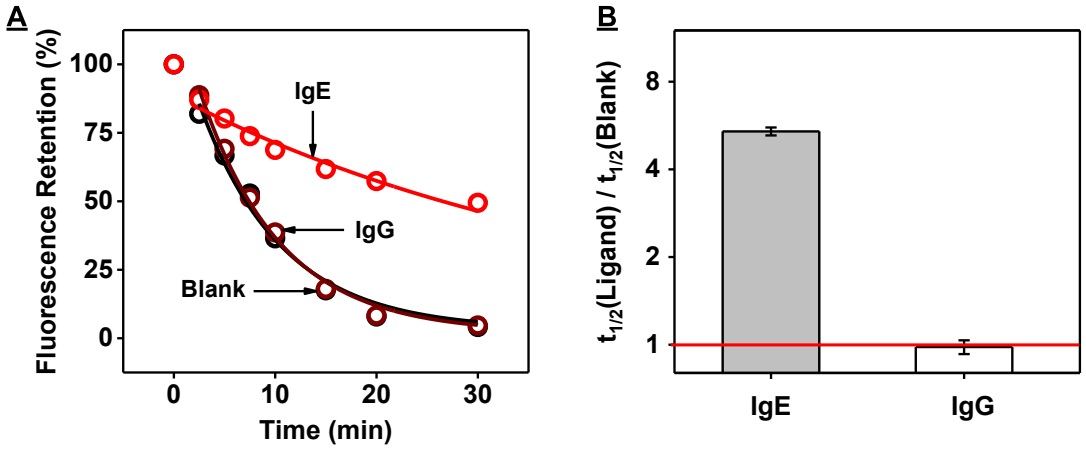

Figure S28. Exonuclease-based fluorescence profiling of an IgE-binding aptamer. (**A**) Time-course plot of aptamer digestion by Exo III and Exo I in the absence (black) and presence of 500 nM human IgE (red) or IgG (brown). (**B**) $t_{1/2}$ ratios calculated from plot A. The y-axis is $\log_2$ scaled. The red line indicates a $t_{1/2}$ ratio of 1, which means there was no inhibition of aptamer digestion.

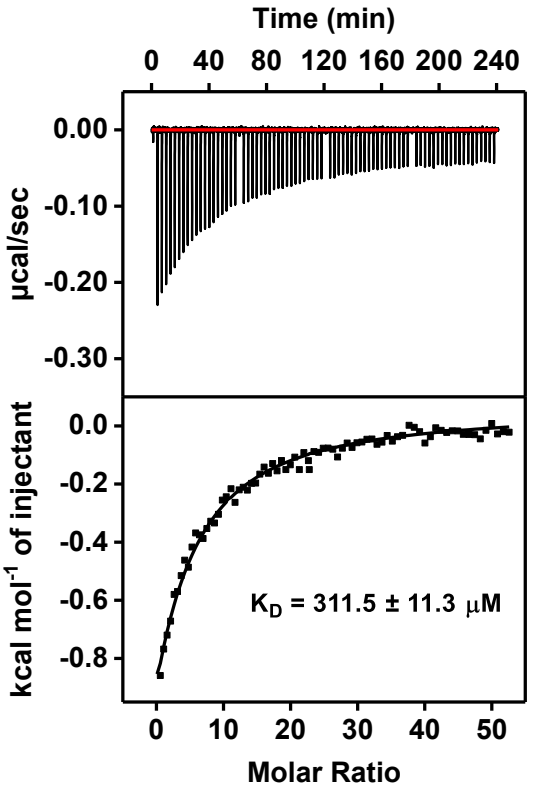

Figure S29. Characterization of ligand-binding affinity of a recently published ADE-binding aptamer (A10-excised) (*Chem. Sci.*, **2020**, *11*, 2735-2743) to ADE using ITC at room temperature. Top panel displays the heat generated from each titration of ADE to the aptamer. Bottom panel shows the integrated heat of each titration after correcting for the heat of dilution of the titrant. Buffer: 10 mM Tris-HCl, pH 7.4, 20 mM NaCl and 1.5 mM $MgCl_2$.

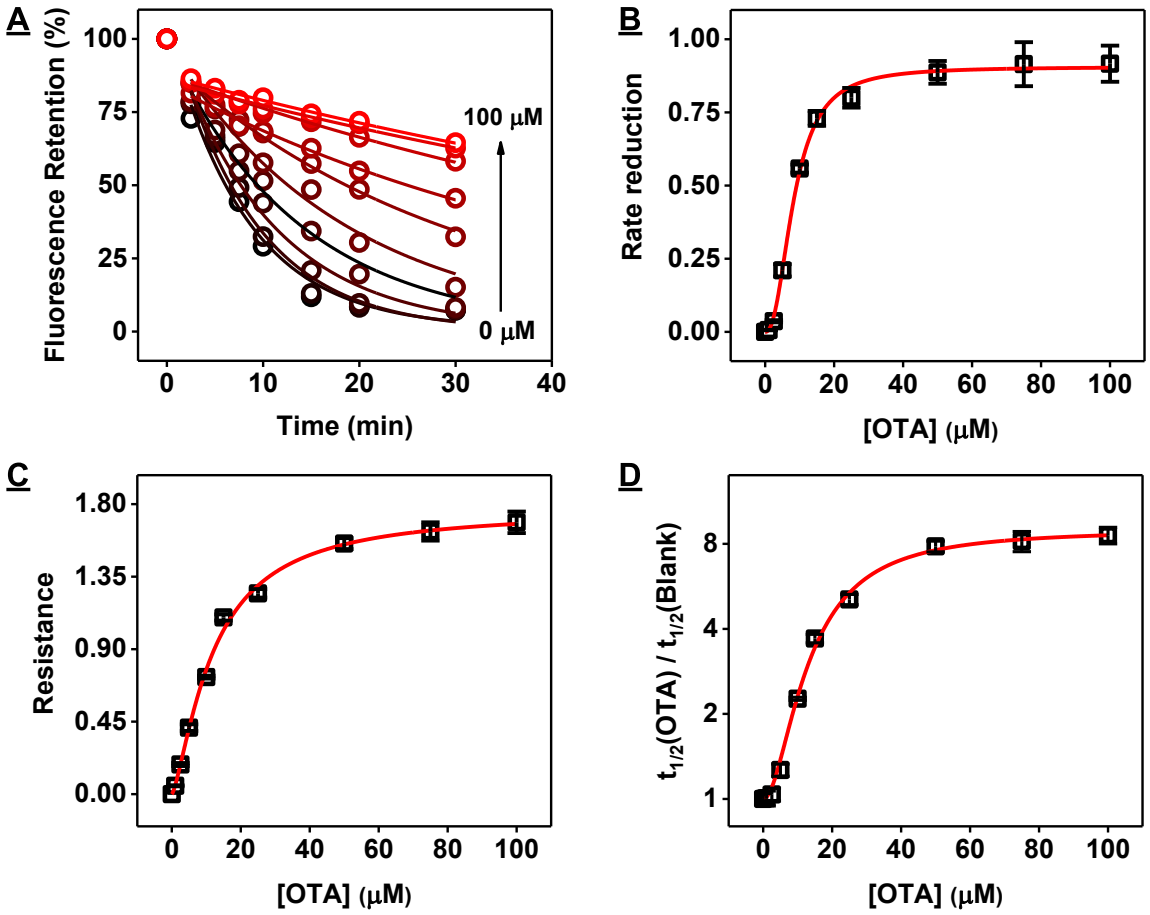

Figure S30. Characterization of OBA3 affinity for OTA using the exonuclease digestion assay. (**A**) Fluorescence time-course of the digestion of 1 µM OBA3 in the absence and presence of 0, 1, 2.5, 5, 10, 15, 25, 50, 75 and 100 µM OTA (indicated by black to red color gradient). Data analysis performed by plotting (**B**) reduction in first-order reaction rate of aptamer digestion ($1 - k_{OTA}/k_{blank}$); (**C**) the aptamer's resistance to digestion based on the area under the curve (AUC) of fluorescence digestion plots ($(AUC_{OTA}/AUC_{blank}) - 1$); and (**D**) $t_{1/2}$ ratio at each ligand concentration.